Journal of King Saud University – Science 33 (2021) 101434

Contents lists available at ScienceDirect

Journal of King Saud University – Science

journal homepage: www.sciencedirect.com

Original article

Therapeutic potential of galactosamine-modified hollow silica nanoparticle for improved drug targeting to liver cancer

Lei Shi [a], Vidya Devanathadesikan Seshadri [b], Mohammed Mustafa Poyil [c], Mohammed H. Karrar Alsharif [c], Rasiravathanahalli Kaveriyappan Govindarajan [d,*], Young Ock Kim [e], Sae Won Na [f], Hak-Jae Kim [e,*], Gamal A. Gabr [b], Randa Mohammed Zaki [g]

[a] Department of Hepatology, Xi'an Hospital Of Traditional Chineses Medicine, Xi'an, Shaanxi 710021, China
[b] Department of Pharmacology and Toxicology, College of Pharmacy, Prince Sattam bin Abdul Aziz University, Al Kharj, Saudi Arabia
[c] Department of Basic Medical Sciences, College of Medicine, Prince Sattam bin Abdul Aziz University, Al Kharj, Saudi Arabia
[d] Division of Biotechnology, School of Agro-Industry, Faculty of Agro-Industry, Chiang Mai University, Mae-Hia, Chiang Mai 50100, Thailand
[e] Department of Clinical Pharmacology, College of Medicine, Soonchunhyang University, Cheonan, Republic of Korea
[f] The Comfort Animal Hospital, Sungbuk-gu, Soonginro-50, Seoul, Republic of Korea
[g] Department of Pharmaceutics, College of Pharmacy, Prince Sattam Bin Abdulaziz University, Al-Kharj, Saudi Arabia

ARTICLE INFO

Article history:
Received 2 December 2020
Revised 1 April 2021
Accepted 1 April 2021
Available online 8 April 2021

Keywords:
Hollow mesoporous silica nanoparticle
Hepatocellular carcinoma
Nimbin
Polyethyleneimine

ABSTRACT

Present state-of-the-art focusing on the formulates multifunctional hollow mesoporous silica nanoparticles (HMSNs) represent a reservoir for encapsulating warhead of active entail Nimbin (NB) into the hollow core and the surface modified by PEI-PLA by electrostatic interaction. The fabricated hollow mesoporous silica (HMSN) nano drug framework is amended with polyethyleneimine (PEI)-poly lactic acid (PLA) with carboxylic group terminus used to tag liver tumour-targeting agent galactosamine (GAL). Thus, with surface modified HMSNs capable of internalization into cancer cells, the ability of NB to discharge into cancerous cells influenced by environmental pH value. The emerging active ingredient firmly suppresses the expression of the P13/Akt pathway to induce apoptosis by creating DNA fragmentation, caspase activation and reactive oxygen species (ROS). The released NB drug significantly improves cancer cell killing in vitro. As a result, the analysis revealed a drug delivery platform by NB to understand the cancer cell targeting strategy.

1. Introduction

Hepatocellular carcinoma (HCC) is the most prevalent fatality disease with a grim prognosis worldwide. There are currently several therapeutic options open to restore HCC, including liver resection, liver transplantation, and chemotherapy. New nano drug delivery systems are the most effective technique for optimizing HCC care to achieve adequate HCC therapy. This nano drug device has a small size (1–100 nm) and a wide surface area used to entrap drug moieties either in their core, on the surface, or both regions (Baig et al., 2019). Such nanodrug delivery mechanisms include liposomes, metal oxide nanoparticles (NPs), polymeric and inorganic NPs that can use substantially to distribute anti-cancer drugs and improve the drug circulation time in the blood (Chenthamara et al., 2019; Din et al., 2017). In treatment for cancer, HMSN are some of the tremendous appealing drug carriers used in cancer therapy; their supremacy has also been effectively formed, which include high surface area, excellent biocompatibility, and high mesoporous volume, allowing a large number of drugs to be encapsulated and encapsulated into their mesoporous channels and hollow interiors. In specific, HMSN has seen a more splendid recital for drug delivery due to highly permeable intact porous shells, unique large hollow cavities, well-defined, and controlled particle morphology. Recent research has shown that HMSN could increase the loading ability of doxorubicin by 100% relative to standard mesoporous silica nanoparticles (MSNs) thus reducing the toxic impact of drug carriers (Shen et al., 2011). Besides all the advantages of MSNs, HMSNs must be especially remarkable in the drug

* Corresponding authors.
E-mail addresses: biogovindarajan@gmail.com (R. Kaveriyappan Govindarajan), hak3962@sch.ac.kr (H.-J. Kim).
Peer review under responsibility of King Saud University.

Production and hosting by Elsevier

https://doi.org/10.1016/j.jksus.2021.101434

delivery systems owing to their adequate amount of drug storage in the central cavity structure. A lower amount of HMSNs can have beneficial therapeutic results as compared with MSNs. As a result, it deduces the potential accumulation of materials in a host body regarding potential biosafety (Florek et al., 2017; Li et al., 2011). Therefore, several studies have shown that the fabricate of HMSNs is noteworthy in drug delivery systems.

A plant-based active molecule of Nimbin (NB) is isolated from *Azadirachta indica* leaves, deducing the expression rates of various signalling molecules such as RAF, Cyclin D1, p-Erk, RAS, and RAS in both MDA MB-231 and MCF-7 breast cancer cells. Thus, the active constituents as a potential cancer progression inhibitor isolated from the leave extract of neem can target diverse signalling molecules involved in complicating the disease. Distribution of anticancer agents into cancer cells by nanoparticles guarantees the deduction in the therapeutic dosage, strengthens the sustainable drug release, reduces the undesirable toxicities, and prevents the decomposition of drug molecules. Various liver-targeting ligands have been applied to the surface of the nanosystem for successful targeting to resolve the issue of poor target performance and increased permeability and retention effect (EPR) (Rizvi and Saleh, 2018; Navya et al., 2019). Galactose (GA) has the potential to penetrate HCC cells with asialoglycoprotein (ASGP) receptor expression. Notably, the ASGP receptor is skilled in identifying galactose-glycoproteins and glycoconjugates; consequently, many particles loaded with galactose were employed as nano-drug carrier systems for HCC target therapy. Galactosamine-conjugated poly (-glutamic acid)-poly(lactide) nanosized particles can be engaged as an active targeted drug for liver cancer treatment because galactosamine (GAL) is capable of distinguishing and interacts with the ASGP receptors on the exterior of HCC cells (D'Souza and Devarajan, 2015; Li et al., 2016).

Present state-of-the-art focused on developing NB loaded HMSNs for the intelligent delivery of model anti-cancer drugs to liver cancer. The small siliceous pores and central cavity framework of HMSNs were loaded with NB, and then the outer layer of the drug-loaded HMSNs was decorated by PEI-PLA. Besides, HMSN-PEI-PLA was subsequently capped with GAL on the surface of nanoparticles. The GAL significantly improves the NB loaded HMSN-PEI-PLA uptake by liver cancer cells through the interaction between the GAL and ASGP receptors. The PEI-PLA gets detaches at acidic pH, which allows the steady leakage of NB, and then the discharged NB act as a growth suppression and DNA disruptor. The biological properties such as intracellular drug delivery, active targeting, subcellular localization, and *in vivo* treatment worth of GAL-HMSN-PEI-PLA have been executed.

2. Materials and methods

2.1. Materials

Tetraethyl orthosilicate (TEOS), 3-Aminopropyltriethoxy silane (APES), Polyethyleneimine (PEI, Mw ~ 2,000), Polylactic acid (PLA, Mw ~ 60,000), phosphate-buffered solution (PBS, pH 7.4), Cetyltrimethylammonium bromide (CTAB), Ammonia solution (NH_3, 25–28%), Hyclone trypsin and Fetal bovine serum (FBS) were acquired from Sigma Aldrich.

2.2. Synthesis of hollow mesoporous silica nanoparticle

HMSN was fabricated by following a modified Stober method. Typically, 2 mL of TEOS was quickly loaded into the reaction mixture consisting of 24.66 mL of ethanol, 3.33 mL of deionized (DI) water, 300 μL of APES, and 1.0 mL of aqueous solution ammonium (25–28%). The reaction mixture was agitated for 1 h; it appears as a white colloidal suspension. The colloidal suspension was then centrifugally separated and washed with ethanol three times. Subsequently, the 50 mL of CTAB (12 mg/mL) solution was introduced and further agitated for 30 min. After the reaction time, adding 1g of Na_2CO_3 and was stirred for 37 °C/24 h. Afterwards, the product was acquired by centrifugation at 10,000 rpm for 20 min and washed three times with ethanol. The CTAB was eliminated from the sample was calcination at 550 °C/6 h. Lastly, the sample was dispersed in 80 mL of acetone and refluxed at 80 °C/24 h. Lastly, The extraction procedure was continued three times to eliminate surfactant completely, and the final products were obtained and washed with DI water (Rayappan et al., 2017).

2.3. Preparation of GAL-HMSN-PEI-PLA

The surface modification of HMSNs was divided into four steps. Briefly, there are two kinds of PEI anchored on the surface of HMSNs. The obtained PEI-PLA incorporated into the pore wall of the HMSNs by the following procedure. For this, 0.50 g of HMSN-NH_2 was refluxed with 50 mL of anhydrous dimethylformamide (DMF) comprising PEI-PLA at 1:1 M ratio for12 h. The products were obtained through the centrifugation process and tumour targeting agents GAL was anchored by agitated continuously for 20 min in a dynamic atmosphere of nitrogen. The received product after the centrifugation describes as GAL-PEI-PLA-HMSN.

2.4. NB loading and release

The NB was packed into the internal cavity of HMSNs for an estimate release profile of drug moiety. For this, 5 mg/ml of NB was dissolved into 20 mL of DI water containing 50 mg of HMSNs. Then, the blended mixture was agitated continuously for 24 h, and NB loaded GAL-HMSN-PEI-PLA was attained by centrifugation (10,000 rpm for 20 min) and thoroughly washed to eliminate the unbound NB adsorbed on the NPs surface. The supernatant was then filtered over a 0.22-μm filter by the purification process and measuring the absorbance at 214 nm using UV–Vis spectroscopy. Drug loading efficiency (wt %) = (mass of NB in the HMSN)/(mass of HMSN loaded with NB) (Schwarzl et al., 2017). The EE% = (mass of NB achieved in the HMSNs/mass of the feeding NB × 100).

Two milligrams of NB-loaded GAL-HMSN-PEG-PLA was dispersed in 1 mL of PBS at different pH (7.4, 6.8, and 5.5), and the solution was poured into a dialysis bag (7000-MW cut-off) and kept in 50 mL of PBS, at certain time intervals; a portion of discharge medium (1 mL) was used to evaluate discharge rate of NB by UV–vis spectroscopy at 214 nm (n = 3).

2.5. Characterization

The particle morphology and size of GAL-HMSN-PEI-PLA was investigated using high-resolution transmission electron microscopy (HR-TEM, JEOL JEM-2100). For Field-emission scanning electron microscope (FE-SEM) analysis, a small amount (4 μL) of the diluted sample was poured on a silicon wafer and then dried at 37 °C to remove moisture. The sample was analyzed using an FE-SEM (Quanta 200 FEG). Fourier transform infrared (FT-IR) spectrum was measured in transmission mode with a scanning range of 4000–400 cm^{-1} (Nicolet 6700 FTIR spectrophotometer, Thermo Fisher, USA.). The Brunauer-Emmett-Teller (BET) analysis was used to measure the surface areas of formulated nanomaterials. Particle size distribution and surface charge were evaluated on Nano-ZS (Malvern).

2.6. Cell culture and maintenance

The liver cancer cell line (Hep G2) Purchased from NCCB Pune, India. Hep G2 cells ($2X10^4$ cells/cm^2) were grown in high glucose DMEM medium and the media was supplied with antibiotics such as streptomycin and penicillin at a 100 U/mL concentration and kept in a humidified atmosphere (5% CO_2 at 37 °C). The fresh medium was replaced every two days.

2.7. In vitro cytotoxicity assay

The cytotoxic impact of bare nanocarrier was studied using HBL-100 normal breast cells at the concentration ranging from 0.5 to 64 μg/mL and the NB loaded GAL-HMSN-PEI-PLA on HepG2 cells was assessed using 3-(4,5- Dimethylthiazol-2-yl)-2,5-diphe nyltertrazolium bromide (MTT) assay for 24 h at different concentrations (5–80 μg). Briefly, HepG2 (1×10^5/well) cells were grown in 96-well plates; after reaching a confluence up to 90%, the Hep G2 cells were treated with NB, HMSN-PEI-PLA, NB loaded HMSN-PEI-PLA, and NB loaded GAL-HMSN-PEI-PLAand incubated at 37 °C for 24 h. Afterwards, 200 μL of MTT was poured into each well contains Hep G2 cells with drugs. After the 30 min incubation, the medium of each cell was discarded and washed with 300 μL of DMSO. Then, the OD value of the MTT was measured at 540 nm by a microplate reader to obtain the percentage of cell viability.

2.8. Western blotting

HepG2 cells were treated with NB loaded GAL-HMSN-PEI-PLA, then the treated cells were homogenized and collect the supernatant to assess the protein expression by SDS-PAGE. The separated protein onto the gel was then moved to a polyvinylidene difluoride membrane. Each blot was blocked and incubated with specific primary antibodies, include PI3-K, AKT, Ras, caspase-9, Bcl-2, Bax, cytochrome *c*, caspase-3 and β-Actin. The primary antibody incubated membrane was rinsed with buffer and incubation with secondary antibody at room temperature.

2.9. Detection of reactive oxygen species

ROS generation was evaluated in NB loaded GAL-HMSN-PEI-PLA treated HepG2 cells at IC_{50} concentration for 24 h. Then, 200 μL of 5-(and-6)-chloromethyl-2′,7′-dichlorodihydrofluorescein diacetate (DCF-DA, 1 mg/mL) was used to stain the treated Hep G2 cells and incubated for 30 min. A Nikon Eclipse fluorescence microscope used to evaluated subcellular ROS generation. The fluorescent intensity was evaluated at 540 nm using a fluorescence plate reader (Kwon et al., 2019).

2.10. Statistical analysis

The value of every experiment was individually carried out three times (n = 3), and the data were estimated by a mean ± standard error and Student's *t*-test. Also, the impact was statistically measured if $P_{\text{-value}} \leq 0.05$.

3. Result

Due to their excellent surface area, good biocompatibility, and substantial drug retention capacity, HMSNs are considered a talented cancer treatment drug delivery system. Herein, the co-condensation process used to formulate HMSNs using TEOS as a source of silica, and a small quantity of NH_3 was used as a catalyst. The large internal cavity and pore shell of HMSN is encapsulated with NB used as an antineoplastic agent. The surface of the HMSN-loaded NB was then filled with the PEI-PLA organic polymer moieties by electrostatic interaction. Drug loaded HMSN has been functionalized with PLA consisting of carboxyl groups used to label GAL as a targeting agent for liver cancer cells, resulting in GAL-HMSNs capable of targeting only active cancer cells (Fig. 1), which has been interacting with over-expression ASGP receptors on the surface of liver cancer cells.

The electron microscopic study was investigated to determine the structure, morphology, and size of the HMSN formulated. FE-SEM and TEM exhibited well-defined single-dispersed spherical shaped HMSNs with a typical diameter of 55 ± 10 nm (Fig. S1) and Gal-NB-HMSN-PEI-PLA comprising of a thin outer layer of the shell, suggesting the existence of organic fractions that fully cover the core area of HMSN. It is recommended that the Gal-NB-HMSN-PEI-PLA nanoparticles can modify their microstructure since the conjugations of functional molecules. The massively higher intensity within the nanoparticle intensity variance between the core and the surface area of the HMSNs confirmed the existence of hollow structure. As shown in Fig. S1, the size distribution and mean hydrodynamic diameter HMSNs in DI water was evaluated by dynamic light scattering (DLS) at 37 °C. The bare HMSN was to be 70.5 nm with 0.61 polydispersity index, which allows a high dispersion of HMSNs in DI water. FTIR results con-

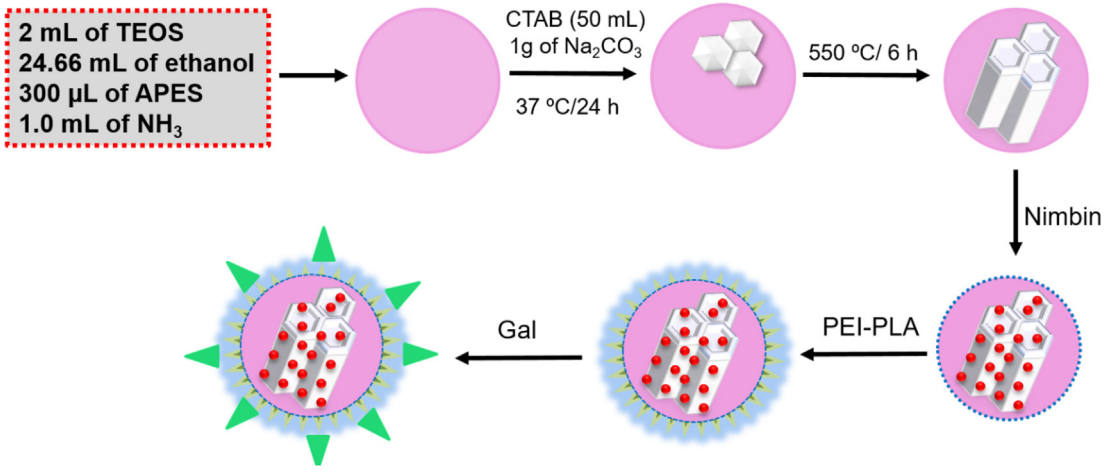

Fig. 1. Schematic illustrates describing the drug loading ability in Gal-NB-HMSN-PEI-PLA materials that display the release of drug molecules activity in the tumor subcellular region for enhanced cancer therapy.

firmed the spectra of HMSN and HMSN-PEI-PLA. The sample has large bands located at around 3300–3500 cm^{-1} (υSi–OH), 1100 (υasym. Si–O–Si), and 460 (δO–Si–O), occurring because of the organo alkoxysilane in the particles (Mishra et al., 2021; Mishra et al., 2014). The FT-IR spectra of PEI-HMSN revealed the adsorption peak of PEI at 1380 cm^{-1}. Also, the peak at 945 cm^{-1}confirms the stretching vibration of Si-OH has been diminished, proposing that Si-OH groups can interfere with the positively charged group $[-CH_2-CH_2-NH_2+-]_n$ and deduce the Si-OH groups during the adsorption process. The –OH stretching pulse at 3431 cm^{-1}displays the PEI adsorption on HMSN and the presence of C=O vibration of COOH confirmed by a peak at 1730 cm^{-1} identifies the existence of PLA in HMSN-PEI (Liu et al., 2019; Kong et al., 2017; Amani et al., 2019).

In Fig. 2, the zeta potential of HMSN, HMSN-PEI, HMSN-PEI-PLA, and Gal-HMSN-PEI-PLA was diluted in double-distilled water. The zeta potential of HMSN was −22.6 mV. After the outer surface of HMSN alteration with PEI, it was noted to be +26.4 mV caused by the existence of amine groups in the backbone of PEI. The surface charge of HMSN-PEI-PLA was to be calculated −20.3 mV, and this alteration was mostly owed to the existence of COO- groups in the PLA of HMSN-PEI-PLA. The zeta potential of Gal-HMSN-PEI-PLA, which is seen to be 20.3 mV showing the presence of positively charged amino groups on Gal-HMSN-PEI-PLA. It is generally recognized that cationic nanoparticles get a strong binding to the anionic cell surface, which leads to elevated endocytosis.

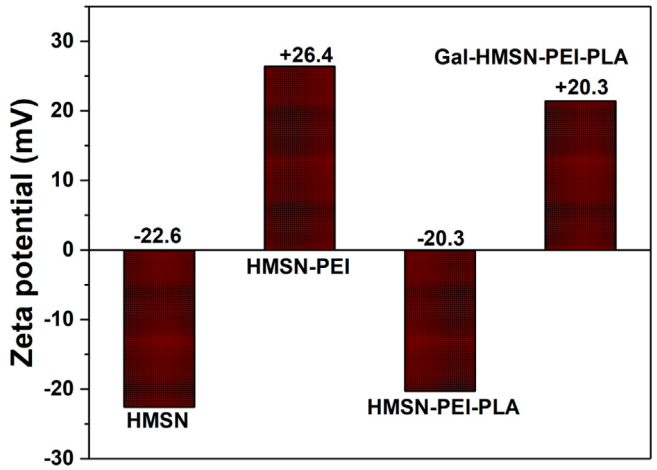

Fig. 2. Zeta potential of fabricated materials such as HMSN, HMSN-PEI, HMSN-PEI-PLA, and Gal-HMSN-PEI-PLA was evaluated at pH 6.8 in DI water.

As seen in Fig. 3, the surface area of HMSN was assessed to be 889.4 cm^2/g by BET analysis. The porosity of HMSN was measured to be 2.6 nm by the BJH method. The mesoporous structure and pore volume was decided by the alkyl chain length of the CTAB. The pore volume was calculated to be 0.77 cm^2 g^{-1}. HMSN with type IV isotherm curves reveals the sufficient indication of the mesoporous formation (Rayappan et al., 2017; Murugan et al., 2017).

The entrapment of the NB was conducted similarly and explored by UV–Vis, which stated to be a sensitive approach for the analysis of entrapment mechanisms. The NB entrapment was achieved by incubation of the HMSN-PEI-PLA in the NB solution for 5 h, which was placed into polymer layers and within the HMSNs. The EE% was calculated to be 83.3% of the NB in the HMSN-PEI-PLA. In other words, the entrapment of NB ~ 0.26 mg per mg of the powder sample of HMSNs. Owing to its hydrophobic aspect, NB often physically tethered in the porous wall of HMSN and functionalized polymeric network (PEI-PLA) of the HMSN shell. The release of NB from the Gal-HMSN-PEI-PLA was studied at pH 7.4 and pH 4.0 of PBS solution. The experimental product was kept in an incubator shaker at 37 °C, and then the absorbance value of the supernatant was evaluated at certain time intervals. The discharged was noted for 24 h, as seen in the drug release. Initially, rapid release (~45% of NB) was observed up to 3 h because of the immediate discharge of surface-bound NB through the concentration gradient mediated diffusion cycle. A maximum discharge of NB was noted to be 78% at pH 4.0 at 24 h. It shows that HMSNs had a high loading power, which may be credited to the electrostatic interaction between the hydrophobic NB and the negatively charged core of HMSN with a hydroxyl group (-OH). Premature release of NB from Gal-HMSN-PEI-PLA at pH 7.4 was observed to be very low, which deduce the undesired side effects on healthy tissues during the nanocarriers in blood circulation. In addition, the NB-loaded Gal-HMSN-PEI-PLA arrived at the tumour region, the targeting properties of Gal could be engaging with ASGP receptors on the exterior of Hep G2 cells, which facilitated the absorption of nanoparticles by cancer cells and stimulated the hydrolysis of PEI-PLA polymers triggered by intracellular NB (Choudhury et al., 2016; Mattos et al., 2017; Murugan et al., 2019).

The treatment of HBL-100 by free HMSN-PEI-PLA at different concentrations in the range of 0.5–64 μg/mL showed no significant deduction in HBL-100 cell viability in 24 h incubation. The results displayed that the bare nanocarriers revealed minimal toxic effects

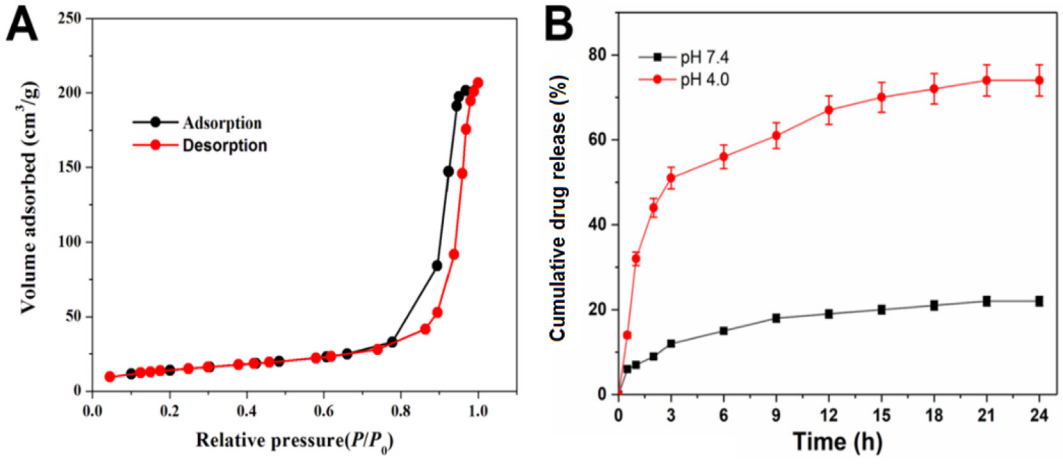

Fig. 3. (A) N_2-sorption isotherms authenticates the porous feature of fabricated HMSNs and (B) release profile of NB loaded Gal-HMSN-PEI-PLA was observed the physiological pH (7.4) and endo/lysosomal pH (4.0) at 37 °C. Error bars provide based on mean ± SD of n = 3.

on normal cells, indicating the biocompatible nature of nanoformulations (Fig. 4).

The cytotoxic effects of free NB, NB-HMSN-PEI-PLA, and Gal-NB-HMSN-PEI-PLA on human liver cancer cell lines (HepG2) were tested by MTT assay. Treatment of cancerous liver cells by free NB, NB-HMSN-PEI-PLA, and Gal-NB-HMSN-PEI-PLA at various concentrations (5–80 μg/mL) for 24 h, which reveals the cytotoxicity occurred in a dose-dependent manner (Fig. 5). The finding suggests that NB free drug has been shown to decrease significantly the viability of HepG2 cells. Furthermore, treatment with NB-HMSN-PEI-PLA displayed a surprising deduction in the proliferation of the HepG2 cell line. The findings show that the loading of the drug into HMSNs raised its cytotoxic activity relative to the free NB. On the other hand, treatment with Gal-NB-HMSN-PEI-PLA found that the cytotoxic activity was more potent in HepG2 cells (88.06%), implying increased expression of the ASGP receptor in HepG2 cells. The disparity in cytotoxicity was primarily attributed to the capacity of Gal-NB-HMSN-PEI-PLA to kill cancer cells that express ASGP receptors. Gal-NB-HMSN-PEI-PLA strongly binds to highly expressed ASGP receptors in HepG2 liver cancer cells, resulting in an increased rate of receptor-mediated endocytosis cellular uptake. Furthermore, the findings suggest that Gal-NB-HMSN-PEI-PLA was more easily internalized across an endocytosis system than other HMSNs owing to the possession of the positively charged PEI and Gal as a liver cancer cell-targeted moiety. Upon internalization, Gal-NB-HMSN-PEI-PLA releases NB in the cytoplasm and enhances the therapeutic benefit on the HepG2 cell at IC_{50} concentration of 20 μg/mL (Puri et al., 2018; Nguyen et al., 2015).

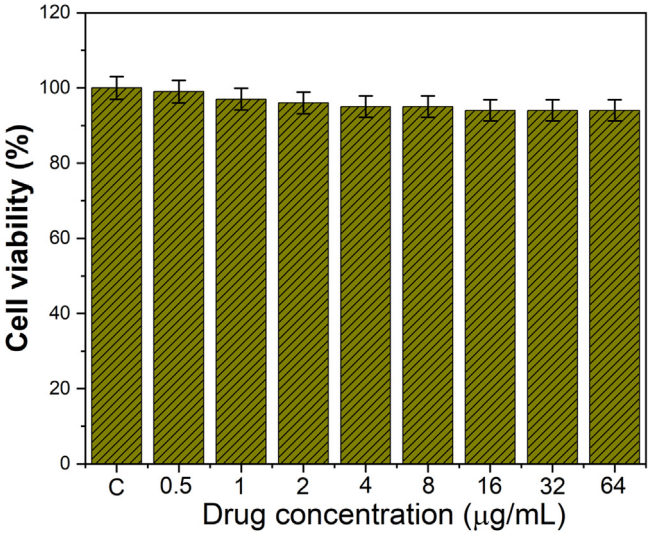

Fig. 4. Cell viability of HMSN-PEI-PLA using normal breast cells (HBL-100) by MTT assay.

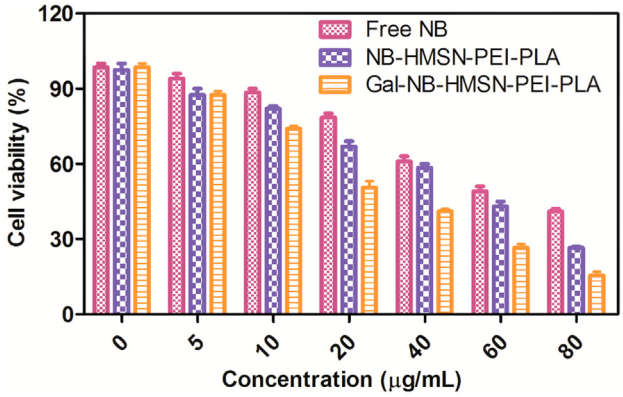

Fig. 5. Cell viability was evaluated by MTT assay. HepG2 cells treated with free NB, NB-HMSN-PEI-PLA, and Gal-NB-HMSN-PEI-PLA for 24 h at numerous concentrations. The viability of HepG2 cells treated with Gal-NB-HMSN-PEI-PLA was assessed to be considerably decreased in association to cells treated with free drugs and NB-HMSN-PEI-PLA.

The impacts of NB-HMSN-PEI-PLA and Gal-NB-HMSN-PEI-PLA on nuclear condensation, nucleic acid disruption, and HepG2 cell morphology were examined by fluorescence microscopy (Fig. 6). The DAPI fluorescent dye is readily formed dual-stranded DNA adducts, and the DAPI dye revealed the nuclear condensation of apoptotic cells. The NB-loaded HMSN-PEI-PLA and Gal-NB-HMSN-PEI-PLA treated cells retain unusual features such as segmented nucleus morphology nucleus chromatin and entirely fractured nuclear bodies, and these characteristics signify the likelihood of induction of apoptosis. The cancer cells treated with NB-HMSN-PEI-PLA and Gal-NB-HMSN-PEI-PLA (IC_{50} 20 μg/ml) impaired cell growth was noted. Then, the Gal-NB-HMSN-PEI-PLA has an increased rate of anti-proliferative effects than NB-HMSN-PEI-PLA. These findings indicate that Gal-NB-HMSN-PEI-PLA could effectually prevent the spread of cancer cells, as stated in the previous research (Murugan et al., 2020a, 2020b). The above results revealed that Gal-NB-HMSN-PEI-PLA effectively interacts with ASGP receptors on HepG2 cells, resulting in the release of NB in the cytoplasm and nucleus, and successively increases the apoptotic effect by DNA damage and mitochondrial dysfunction (Li et al., 2019; Murugan et al., 2020a, 2020b).

Fluorescent markers such as AO and EtBr are used to analyze the categories of living and dead cells. AO is a cationic dye that is able to penetrate the cell membrane and responds by binding or electrostatic contact with DNA and RNA (Fig. S2). The AO can penetrate into both live and dead HepG2 cells because of its lower molecular weight. Although EtBr is an intercalating fluorescent product that can bind with nucleic acid (DNA), only impermeable into the dead cell membrane because of its more considerable molecular weight. The presence of EtBr thus determines the popu-

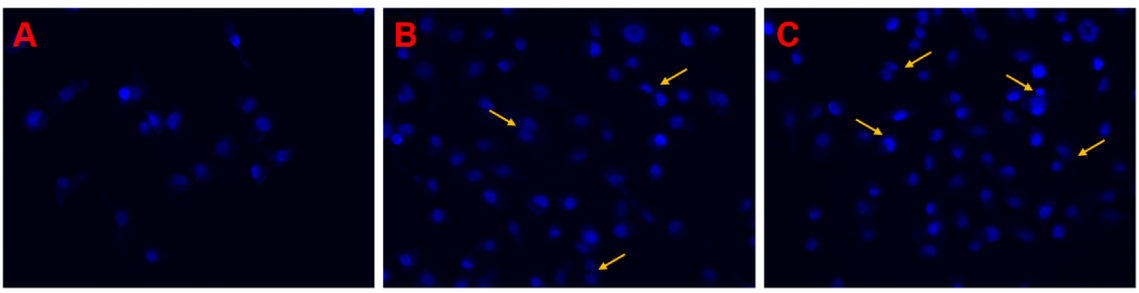

Fig. 6. Fluorescence images (400x magnifications) of DAPI stained HepG2 cells treated with different nanoformulations (A) Control, (B) NB-HMSN-PEI-PLA, and (C) Gal-NB-HMSN-PEI-PLA for 24 h. The treated cancer cells displayed abnormalities in the nucleus, representative of the induction of apoptosis.

lation of apoptotic cells whose membrane was disrupted and showed purple. Following treated with Gal-NB-HMSN-PEI-PLA, only 5% of the AO positive cells can be observed in green colour. Interestingly, after treatment with Gal-NB-HMSN-PEI-PLA, nearly 95% of the HepG2 cells stain for EtBr appeared in red or orange colour, suggesting increased anti-cancer activity due to nanoparticle-mediated directed chemotherapy effect. The orange colour in the overlaid images attributed to the AO (green) and EtBr (red) mixture fluorescence strength, suggesting apoptosis of the HepG2 cells Ansari et al. (2020), Cai et al. (2020), Chen et al. (2020), Dong et al. (2019), Hai et al. (2018), Jafari et al. (2019), Liu et al. (2020).

As seen in Fig. 7, control, NB-HMSN-PEI-PLA, and Gal-NB-HMSN-PEI-PLA were used to testify for measuring ROS generation. The fluorescence intensity of DCFH-DA stain was observed in HepG2 cells treated. Of note, 20 μg/ml NB-HMSN-PEI-PLA and Gal-NB-HMSN-PEI-PLA caused ROS generation within 24 h of treatment. The NB-HMSN-PEI-PLA raises ROS levels, while the quantity of ROS generation in control. Through the use of targeting agents,

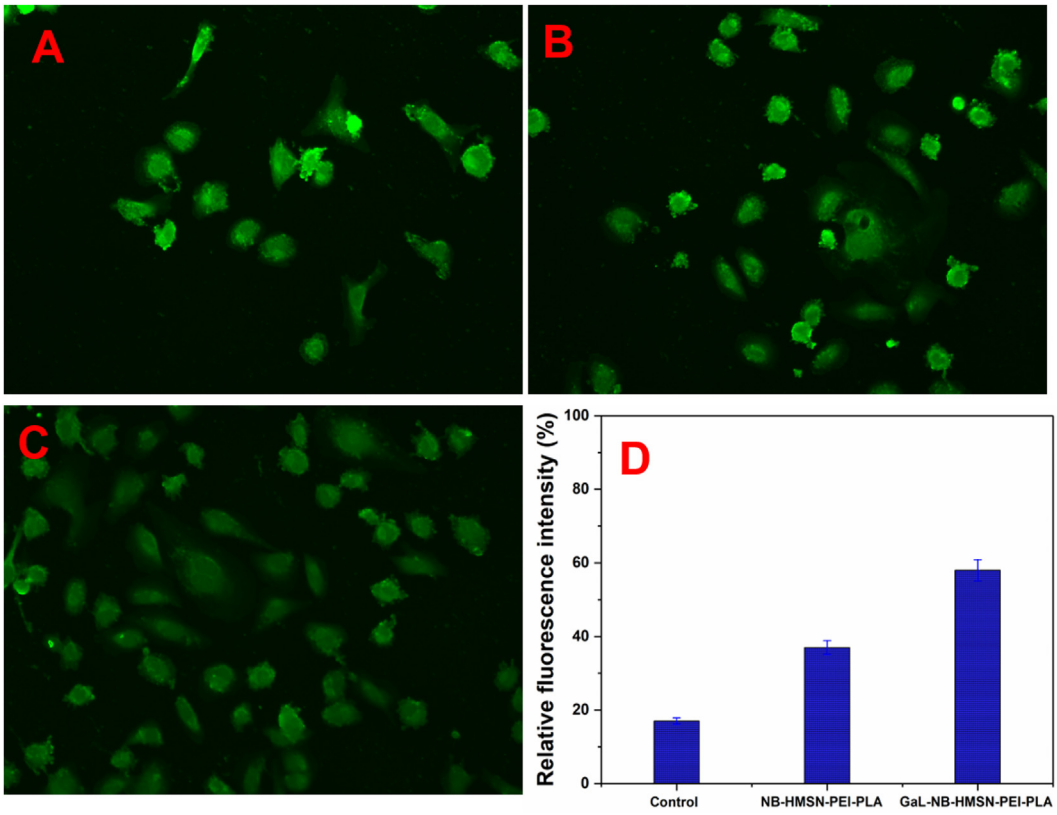

Fig. 7. Fluorescence photographs of HepG2 cells stained with DCFH-DA. (A) Control, (B) NB-HMSN-PEI-PLA, and (C) Gal-NB-HMSN-PEI-PLA on ROS generation and fluorescence intensity of DCF, which is relative rate of ROS generated in the HepG2 cells after treated with different nano-formulation. The data signify mean ± SD $^{*}p \leq 0.05$ was considered statistically significant. Scale bar 400X magnifications.

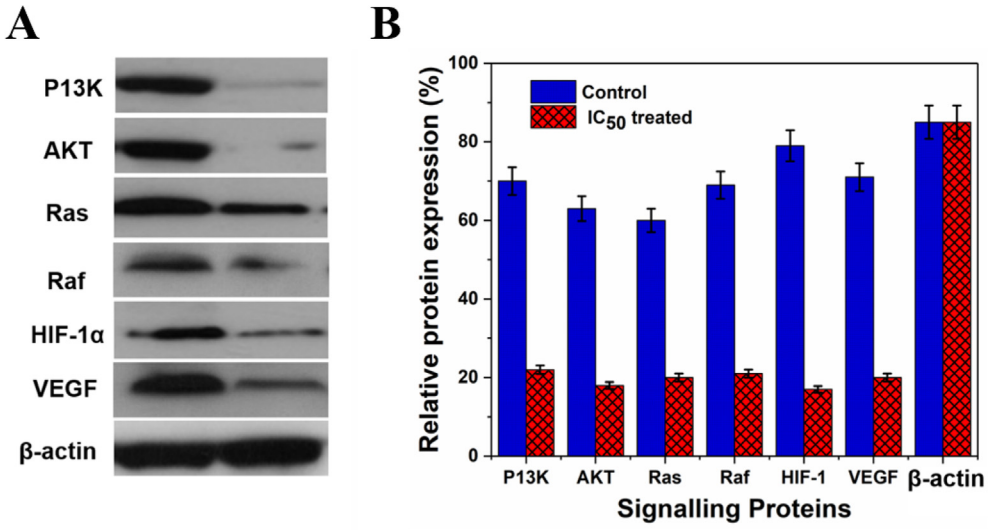

Fig. 8. (A & B) Western blot analysis of the expression level of anti-apoptotic proteins before and after Gal-NB-HMSN-PEI-PLA treatment in HepG2 liver cancer cells. The expression of anti-apoptotic proteins was down-regulated after treated with Gal-NB-HMSN-PEI-PLA, representative the induction of mitochondrial-dependent apoptosis. β-actin served as an internal standard.

the intensity of ROS is greatly modified. Therefore, the ROS level was rose in liver cancer cells within 24 h. These findings suggest that the dual agents such as drug and targeted agent in Gal-NB-HMSN-PEI-PLA synergistically increase ROS generation. These findings indicate that Gal-NB-HMSN-PEI-PLA mediated NB dispersed into HepG2 cells produce the increased rate of ROS and DNA damage that attributes to apoptosis. As a result, Gal-NB-HMSN-PEI-PLA was considered to be the most useful therapeutic agent to capably induce the ROS to trigger intrinsic apoptotic proteins in HepG2 cells. Then, ROS intensity was measured by fluorescence plate reader (Fig. 7D) in Gal-NB-HMSN-PEI-PLA treated HepG2 liver cancer cells. The development of an elevated rate of ROS, therefore, plays a prominent role in the apoptotic regulation (Kobayashi et al., 2014; Seah et al., 2018; Cho et al., 2019).

Western blot investigation reveals the impact of Gal-NB-HMSN-PEI-PLA on Hep G2 cells on the molecular activation of the apoptotic pathway. The expression profile of the significant anti-apoptotic proteins includes angiogenesis protein (VEGF) and hypoxia protein (HIF-15-007) PI3-K, ERK, AKT, Raf and Ras were assessed. The findings indicated the formulated Gal-NB-HMSN-PEI-PLA is responsible for the downregulation of the above-stated proteins in HepG2 cells (Fig. 8A&B).

On the other hand, the Gal-NB-HMSN-PEI-PLA induces the depolarization in the membrane potential of mitochondria triggers ROS-dependent mitochondrial apoptosis via pro-apoptotic factors activation. The research findings have shown that the down-regulation of anti-apoptotic proteins (AKT, Ras, PI3-K, Raf, VEGF, ERK and HIF-15-007, leads to cell death. Thus, Gal-NB-HMSN-PEI-PLA acts as an essential nanomaterial for activating apoptosis-based molecular activation in hypoxia-conditioned HepG2 cancer cells (Qian et al., 2016; Murugan et al., 2020a, 2020b).

4. Conclusion

The present state of the art clearly proven approach to summarize and discharge a naturally derived product into cancer cells. Hydrophobic drug (NB) as a hydrophobic anti-cancer treatment agent for improved chemotherapy. The Gal-NB-HMSN-PEI-PLA surface was altered with the PEI-PLA polymers, which was loaded with free NB porous, inner, and polymeric layer elements via electrostatic interaction. NB-HMSN-PEI-PLA effectively binds to over-expressed ASGP receptors on HepG2 cancer cells as results of accelerated cellular internalization of nanocarriers via receptor-mediated endocytosis. NB-HMSN-PEI-PLA actively attaches to elevated ASGP receptors on HePG2 liver cancer cells. Upon internalization, Gal-HMSN-PEI-PLA releases NB in the cytoplasm and enhances the therapeutic effect on the HepG2 cells at an IC_{50} concentration of 20 μg/mL. The release was noticed to be 78% for NB at pH 4.0 in 24 h.

In comparison, the release of Gal-NB-HMSN-PEI-PLA drugs used to have preponderant cytotoxicity of liver cancer cells. The formulated Gal-NB-HMSN-PEI-PLA at greater tiers suppress the genomic/proteomic expression of PI3-K, AKT, and Ras, Raf, and ERK, thereby hindering the binding of HIF-15-007 to HIF-1β. In conclusion, the results revealed the functionalized Gal-NB-HMSN-PEI-PLA as a popular flexible drug carrier that could serve as an option in the delivery of drugs for efficacy.

Declaration of Competing Interest

The authors declare that they have no known competing financial interests or personal relationships that could have appeared to influence the work reported in this paper.

Acknowledgement

The authors thank the Deanship of Scientific Research, Prince Sattam bin Abdul Aziz University, Al Kharj, Kingdom of Saudi Arabia.

Appendix A. Supplementary data

Supplementary data to this article can be found online at https://doi.org/10.1016/j.jksus.2021.101434.

References

Amani, A., Kabiri, T., Shafiee, S., Hamidi, A., 2019. Preparation and characterization of PLA-PEG-PLA/PEI/DNA nanoparticles for improvement of transfection efficiency and controlled release of DNA in gene delivery systems. Iran. J. Pharm. Sci. 18 (1), 125.

Ansari, M.Y., Ahmad, N., Voleti, S., Wase, S.J., Novak, K., Haqqi, T.M., 2020. Mitochondrial dysfunction triggers a catabolic response in chondrocytes via ROS-mediated activation of the JNK/AP1 pathway. J. Cell Sci. 133 (22).

Baig, B., Halim, S.A., Farrukh, A., Greish, Y., Amin, A., 2019. Current status of nanomaterial-based treatment for hepatocellular carcinoma. Biomed. Pharmacother. 116, 108852.

Cai, D., Han, C., Liu, C., Ma, X., Qian, J., Zhou, J., Li, Y., Sun, Y., Zhang, C., Zhu, W., 2020. Chitosan-capped enzyme-responsive hollow mesoporous silica nanoplatforms for colon-specific drug delivery. Nanoscale Res. Lett. 15, 1–13.

Chen, K., Jiao, J., Xue, J., Chen, T., Hou, Y., Jiang, Y., Qian, L., Wang, Y., Ma, Z., Liang, Z., Sun, B., 2020. Ginsenoside CK induces apoptosis and suppresses proliferation and invasion of human osteosarcoma cells through the PI3K/mTOR/p70S6K1 pathway. Oncol. Rep. 43 (3), 886–896.

Chenthamara, D., Subramaniam, S., Ramakrishnan, S.G., Krishnaswamy, S., Essa, M. M., Lin, F.H., Qoronfleh, M.W., 2019. Therapeutic efficacy of nanoparticles and routes of administration. Biomater. Res. 23 (1), 1–29.

Cho, H.Y., Mavi, A., Chueng, S.T., Pongkulapa, T., Pasquale, N., Rabie, H., Han, J., Kim, J. H., Kim, T.H., Choi, J.W., Lee, K.B., 2019. Tumor homing reactive oxygen species nanoparticle for enhanced cancer therapy. ACS Appl. Mater. Interfaces 11 (27), 23909–23918.

Choudhury, R., Majumder, M., Roy, D.N., Basumallick, S., Misra, T.K., 2016. Phytotoxicity of Ag nanoparticles prepared by biogenic and chemical methods. Int. Nano Lett 6 (3), 153–159.

Din, F., Aman, W., Ullah, I., Qureshi, O.S., Mustapha, O., Shafique, S., Zeb, A., 2017. Effective use of nanocarriers as drug delivery systems for the treatment of selected tumors. Int. J. Nanomed. 12, 7291.

Dong, J., Yao, X., Sun, S., Zhong, Y., Qian, C., Yang, D., 2019. In vivo targeting of breast cancer with a vasculature-specific GQDs/hMSN nanoplatform. RSC Adv. 9 (20), 11576–11584.

D'Souza, A.A., Devarajan, P.V., 2015. Asialoglycoprotein receptor mediated hepatocyte Targeting-Strategies and applications. J. Control. Release 203, 126–139.

Florek, J., Caillard, R., Kleitz, F., 2017. Evaluation of mesoporous silica nanoparticles for oral drug delivery–current status and perspective of MSNs drug carriers. Nanoscale 9 (40), 15252–15277.

Hai, L., Jia, X., He, D., Zhang, A., Wang, T., Cheng, H., He, X., Wang, K., 2018. DNA-functionalized hollow mesoporous silica nanoparticles with dual cargo loading for near-infrared-responsive synergistic chemo-photothermal treatment of cancer cells. ACS Appl. Nano Mater. 1 (7), 3486–3497.

Jafari, S., Derakhshankhah, H., Alaei, L., Fattahi, A., Varnamkhasti, B.S., Saboury, A.A., 2019. Mesoporous silica nanoparticles for therapeutic/diagnostic applications. Biomed. Pharmacother. 109, 1100–1111.

Kobayashi, H., Watanabe, R., Choyke, P.L., 2014. Improving conventional enhanced permeability and retention (EPR) effects; what is the appropriate target?. Theranostics 4 (1), 81–89.

Kong, M., Tang, J., Qiao, Q., Wu, T., Qi, Y., Tan, S., Gao, X., Zhang, Z., 2017. Biodegradable hollow mesoporous silica nanoparticles for regulating tumor microenvironment and enhancing antitumor efficiency. Theranostics 7 (13), 3276–3292.

Kwon, S., Ko, H., You, D.G., Kataoka, K., Park, J.H., 2019. Nanomedicines for Reactive oxygen species mediated approach: an emerging paradigm for cancer treatment. Acc. Chem. Res. 52 (7), 1771–1782.

Li, C., Wang, Y., Zhang, H., Li, M., Zhu, Z., Xue, Y., 2019. An investigation on the cytotoxicity and caspase-mediated apoptotic effect of biologically synthesized gold nanoparticles using Cardiospermum halicacabum on AGS gastric carcinoma cells. Int. J. Nanomed. 14, 951.

Li, M., Zhang, W., Wang, B., Gao, Y., Song, Z., Zheng, Q.C., 2016. Ligand-based targeted therapy: a novel strategy for hepatocellular carcinoma. Int. J. Nanomed. 11, 5645.

Li, X., Xie, Q.R., Zhang, J., Xia, W., Gu, H., 2011. The packaging of siRNA within the mesoporous structure of silica nanoparticles. Biomaterials 32 (35), 9546–9556.

Liu, J., Wang, Y., Hao, Y., Wang, Z., Yang, Z., Wang, Z., Wang, J., 2020. 5-Heptadecylresorcinol attenuates oxidative damage and mitochondria-

mediated apoptosis through activation of the SIRT3/FOXO3a signaling pathway in neurocytes. Food Funct. 11 (3), 2535–2542.
Liu, Q., Zhou, Y., Li, M., Zhao, L., Ren, J., Li, D., Tan, Z., Wang, K., Li, H., Hussain, M., Zhang, L., Shen, G., Zhu, J., Tao, J., 2019. Polyethylenimine hybrid thin-shell hollow mesoporous silica nanoparticles as vaccine self-adjuvants for cancer immunotherapy. ACS Appl. Mater. Interfaces 11 (51), 47798–47809.
Mattos, B.D., Rojas, O.J., Magalhães, W.L.E., 2017. Biogenic silica nanoparticles loaded with neem bark extract as green, slow-release biocide. J. Clean. Prod. 142, 4206–4213.
Mishra, A., Melo, J.S., Sen, D., D'Souza, S.F., 2014. Evaporation induced self assembled microstructures of silica nanoparticles and Streptococcus lactis cells as sorbent for uranium (VI). J. Colloid Interface Sci. 414, 33–40.
Mishra, A., Pandey, V.K., Shankar, B.S., Melo, J.S., 2021. Spray drying as an efficient route for synthesis of silica nanoparticles-sodium alginate biohybrid drug carrier of doxorubicin. Colloids Surf. B: Biointerfaces 197, 111445.
Murugan, C., Murugan, N., Sundramoorthy, A.K., Sundaramurthy, A., 2020a. Gradient triple-layered ZnS/ZnO/Ta_2O_5-SiO_2 core-shell nanoparticles for enzyme-based electrochemical detection of cancer biomarkers. ACS Appl. Nano Mater. 3 (8), 8461–8471.
Murugan, C., Murugan, N., Sundramoorthy, A.K., Sundaramurthy, A., 2019. Nanoceria decorated flower-like molybdenum sulphide nanoflakes: an efficient nanozyme for tumour selective ROS generation and photo thermal therapy. Chem. Comm. 55 (55), 8017–8020.
Murugan, C., Rajkumar, M., Kanipandian, N., Thangaraj, R., Vimala, K., Kannan, S., 2020b. Nanoformulated CPMSN biomaterial regulates proinflammatory cytokines to heal wounds and kills drug-resistant bacteria. Curr. Sci. 118, 1583.
Murugan, C., Venkatesan, S., Kannan, S., 2017. Cancer therapeutic proficiency of dual-targeted mesoporous silica nanocomposite endorses combination drug delivery. ACS Omega 2 (11), 7959–7975.
Navya, P.N., Kaphle, A., Srinivas, S.P., Bhargava, S.K., Rotello, V.M., Daima, H.K., 2019. Current trends and challenges in cancer management and therapy using designer nanomaterials. NANO Convergence 6 (1), 23.
Nguyen, H.N., Hoang, T.M.N., Mai, T.T.T., Nguyen, T.Q.T., Do, H.D., Pham, T.H., Nguyen, T.L., Ha, P.T., 2015. Enhanced cellular uptake and cytotoxicity of folate decorated doxorubicin loaded PLA-TPGS nanoparticles. Adv. Nat. Sci.-Nanosci. 6 (2), 025005.
Puri, R., Adesina, S., Akala, E., 2018. Cellular uptake and cytotoxicity studies of pH-responsive polymeric nanoparticles fabricated by dispersion polymerization. J. Nanosci. Nanotechnol 2, 3–16.
Qian, J., Bai, H., Gao, Z., Dong, Y.U., Pei, J., Ma, M., Han, B., 2016. Downregulation of HIF-1α inhibits the proliferation and invasion of non-small cell lung cancer NCI-H157 cells. Oncol. Lett. 11 (3), 1738–1744.
Rayappan, K., Murugan, C., Sundarraj, S., Lara, R.P., Kannan, S., 2017. Peptide-conjugated nano-drug delivery system to improve synergistic molecular chemotherapy for colon carcinoma. ChemistrySelect. 2 (27), 8524–8534.
Rizvi, S.A.A., Saleh, A.M., 2018. Applications of nanoparticle systems in drug delivery technology. Saudi Pharm J. 26 (1), 64–70.
Schwarzl, R., Du, F., Haag, R., Netz, R.R., 2017. General method for the quantification of drug loading and release kinetics of nanocarriers. Eur. J. Pharm. Biopharm. 116, 131–137.
Seah, G.L., Yu, J.H., Koo, B.I., Lee, D.J., Nam, Y.S., 2018. Cancer-targeted reactive oxygen species-degradable polymer nanoparticles for near infrared light-induced drug release. J. Mater. Chem. B 6 (46), 7737–7749.
Shen, J., He, Q., Gao, Y., Shi, J., Li, Y., 2011. Mesoporous silica nanoparticles loading doxorubicin reverse multidrug resistance: performance and mechanism. Nanoscale 3 (10), 4314–4322.